

Climate change appears to contribute distinctively, and consistently, to accumulating range compression among bumblebee species across continents. Experimental relocation of bumblebee colonies into new areas could mitigate these range losses. Assessments of climate change on species' ranges need to account for observations across the full extent of species' latitudinal and thermal limits and explicitly test for interactions with other global change drivers.

REFERENCES AND NOTES

1. C. D. Thomas *et al.*, *Nature* **427**, 145–148 (2004).
2. M. Pacifici *et al.*, *Nat. Clim. Change* **5**, 215–224 (2015).
3. I. C. Chen, J. K. Hill, R. Ohlemüller, D. B. Roy, C. D. Thomas, *Science* **333**, 1024–1026 (2011).
4. J. M. Sunday, A. E. Bates, N. K. Dulvy, *Nat. Clim. Change* **2**, 686–690 (2012).
5. J. M. Herrera, E. F. Ploquin, J. Rodríguez-Pérez, J. R. Obeso, M. B. Araújo, *J. Biogeogr.* **41**, 700–712 (2014).
6. E. F. Ploquin, J. M. Herrera, J. R. Obeso, *Oecologia* **173**, 1649–1660 (2013).
7. B. Sinervo *et al.*, *Science* **328**, 894–899 (2010).
8. M. B. Araújo *et al.*, *Ecol. Lett.* **16**, 1206–1219 (2013).
9. V. Kellermann *et al.*, *Proc. Natl. Acad. Sci. U.S.A.* **109**, 16228–16233 (2012).
10. V. Devictor *et al.*, *Nat. Clim. Change* **2**, 121–124 (2012).
11. D. Goulson, E. Nicholls, C. Botías, E. L. Rotheray, *Science* **347**, 1255957 (2015).
12. S. A. Cameron *et al.*, *Proc. Natl. Acad. Sci. U.S.A.* **108**, 662–667 (2011).
13. I. Bartomeus *et al.*, *Proc. Natl. Acad. Sci. U.S.A.* **110**, 4656–4660 (2013).
14. GBIF, *GBIF Metadata Profile, Reference Guide*, Contributed by E. O Tuama, K. Braak (Global Biodiversity Information Facility, Copenhagen, 2011).
15. P. H. Williams, R. W. Thorp, L. L. Richardson, S. R. Colla, *Bumble Bees of North America: An Identification Guide* (Princeton Univ. Press, New York, 2014).
16. Materials and methods are available as supplementary materials on Science Online.
17. S. A. Cameron, H. M. Hines, P. H. Williams, *Biol. J. Linn. Soc. Lond.* **91**, 161–188 (2007).
18. J. Gehrig-Fasel, A. Guisan, N. E. Zimmermann, *J. Veg. Sci.* **18**, 571–582 (2007).
19. M. L. Forister *et al.*, *Proc. Natl. Acad. Sci. U.S.A.* **107**, 2088–2092 (2010).
20. P. R. Whitehorn, S. O'Connor, F. L. Wackers, D. Goulson, *Science* **336**, 351–352 (2012).
21. T. S. Romdal, M. B. Araújo, C. Rahbek, *Glob. Ecol. Biogeogr.* **22**, 344–350 (2013).
22. C. A. Deutsch *et al.*, *Proc. Natl. Acad. Sci. U.S.A.* **105**, 6668–6672 (2008).
23. S. J. Leroux *et al.*, *Ecol. Appl.* **23**, 815–828 (2013).
24. H. M. Hines, *Syst. Biol.* **57**, 58–75 (2008).
25. P. Rasmont, S. Iserbyt, *Ann. Soc. Entomol. Fr.* **48**, 275–280 (2012).
26. J. M. Sunday *et al.*, *Proc. Natl. Acad. Sci. U.S.A.* **111**, 5610–5615 (2014).
27. K. J. Willis, S. A. Bhagwat, *Science* **326**, 806–807 (2009).

ACKNOWLEDGMENTS

This research was funded by the Natural Sciences and Engineering Research Council of Canada strategic network (CANPOLIN: Canadian Pollination Initiative) and Discovery Grant support and University of Ottawa Research Chair in Macroecology and Conservation to J.T.K. We are grateful to anonymous reviewers whose comments improved this paper and to P. Williams for advice and perspectives during development of the research. All data and supporting scripts are available from Dryad Digital Repository: doi:10.5061/dryad.gf774.

SUPPLEMENTARY MATERIALS

www.sciencemag.org/content/349/6244/177/suppl/DC1
Materials and Methods
Supplementary Text
Supplementary Acknowledgments
Figs. S1 to S4
Tables S1 to S3
References (28–55)

15 January 2015; accepted 21 May 2015
10.1126/science.aaa7031

PLACE CELLS

Autoassociative dynamics in the generation of sequences of hippocampal place cells

Brad E. Pfeiffer* and David J. Foster†

Neuronal circuits produce self-sustaining sequences of activity patterns, but the precise mechanisms remain unknown. Here we provide evidence for autoassociative dynamics in sequence generation. During sharp-wave ripple (SWR) events, hippocampal neurons express sequenced reactivations, which we show are composed of discrete attractors. Each attractor corresponds to a single location, the representation of which sharpens over the course of several milliseconds, as the reactivation focuses at that location. Subsequently, the reactivation transitions rapidly to a spatially discontinuous location. This alternation between sharpening and transition occurs repeatedly within individual SWRs and is locked to the slow-gamma (25 to 50 hertz) rhythm. These findings support theoretical notions of neural network function and reveal a fundamental discretization in the retrieval of memory in the hippocampus, together with a function for gamma oscillations in the control of attractor dynamics.

In the well-known Hopfield model, a network of recurrently excitable neurons stores discrete memories as stable activity patterns (attractors) to which partial patterns are guaranteed to converge, based on synaptic weights reflecting correlations between neurons in the same pattern (“autoassociation”) (1). Sequences of patterns can also be stored, based on weights reflecting correlations between different patterns (“heteroassociation”), but are generally unsustainable because any noise leads to divergence in subsequent patterns. A solution is to combine fast autoassociation for each pattern with slower heteroassociation for successive patterns, allowing each pattern to be corrected via attractor network dynamics before transitioning to the next pattern in the sequence (2, 3). This process should result in “jumpy” sequences that sharpen individual pattern representations before transitioning to successive patterns; however, direct evidence is lacking, due largely to the difficulty of obtaining data from very large ensembles of neurons expressing internally generated sequences recorded at the time resolution of neuronal dynamics.

Hippocampal SWR-associated place-cell sequences (4–10), often termed “replay,” are a unique experimental model in which neurons with well-defined receptive fields are activated outside those receptive fields and in specific temporal sequences corresponding to physical trajectories through space, all while the animal is stationary, and thus in the absence of corresponding sequences of stimuli or behaviors. We recently developed methods to record simultaneously from very large num-

bers of hippocampal neurons (up to 263) with place fields in a single environment (10), and we applied these recording techniques to examine the fine structure of SWR-associated place-cell sequences to investigate the underlying mechanisms of this form of memory expression and explore the circuit-level dynamics of an attractor system in vivo.

We recorded bilateral ensemble activity from dorsal hippocampal neurons (figs. S1 and S2) of five rat subjects across multiple recording sessions as they explored open arenas or linear tracks (Fig. 1, A, B, G, and H). We obtained simultaneous recordings from large populations of hippocampal neurons in each recording session (80 to 263 units per session; mean \pm SEM = 159.2 \pm 11.8 units per session), allowing us to accurately decode spatial information from the hippocampal ensemble activity patterns using a memory-less, uniform-prior Bayesian decoding algorithm (fig. S3) (5, 10). We identified SWRs that encoded temporally compressed spatial trajectories through the current environment (Fig. 1, C to F and I to L, and fig. S4) (10), which we term “trajectory events” rather than “replay” to reflect the observation that SWRs do not always represent a perfect replay of immediately prior behavior but instead reflect a more broad array of spatial paths (8–10). Across all sessions in the open field and linear track, we identified 815 and 564 SWR events, respectively, that met our criteria to be classified as trajectory events.

Consistent with prior reports (5), trajectory events displayed average velocities in a relatively narrow range (Fig. 2A); however, when we examined trajectory events on a finer time scale, we observed discontinuous trajectories, alternating between immobility (in which consecutive decoding frames represented the same location) and rapid movement (in which consecutive frames represented a sequential path of unique positions; fig.

Solomon H. Snyder Department of Neuroscience, Johns Hopkins University School of Medicine, Baltimore, MD, USA.

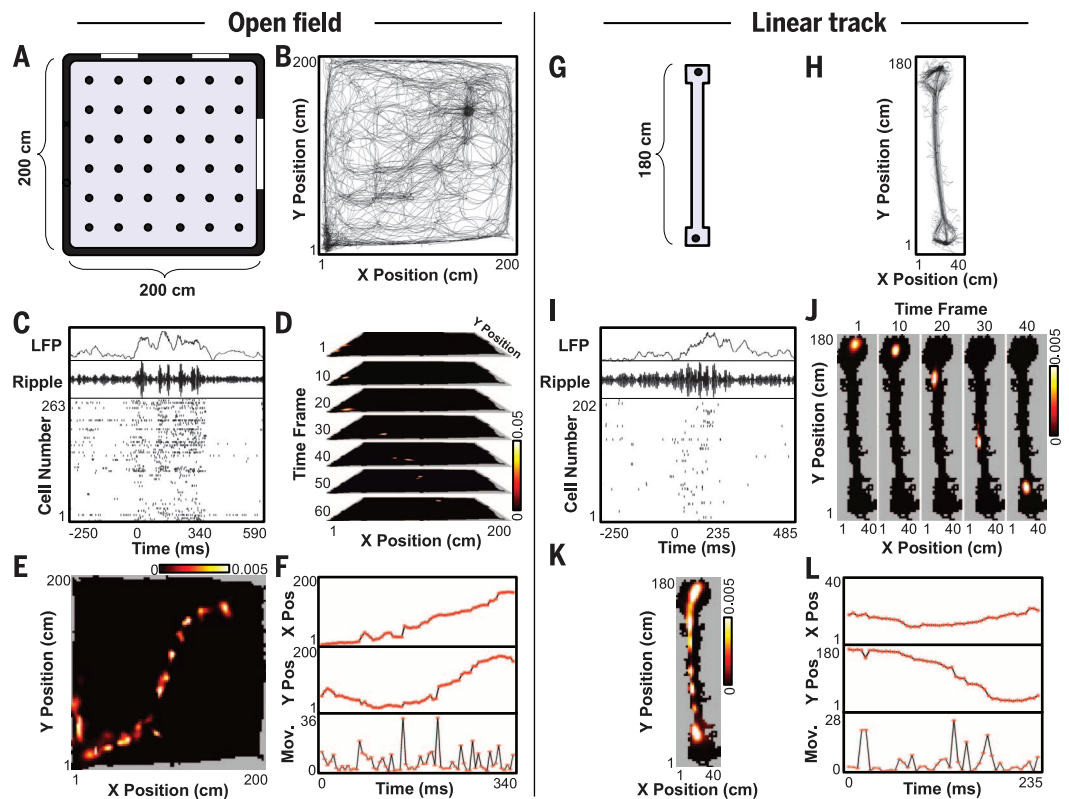
*Present address: Department of Neuroscience, University of Texas Southwestern Medical Center, Dallas, TX, USA.

†Corresponding author. E-mail: david.foster@jhu.edu

Fig. 1. Open arena and linear track trajectory events.

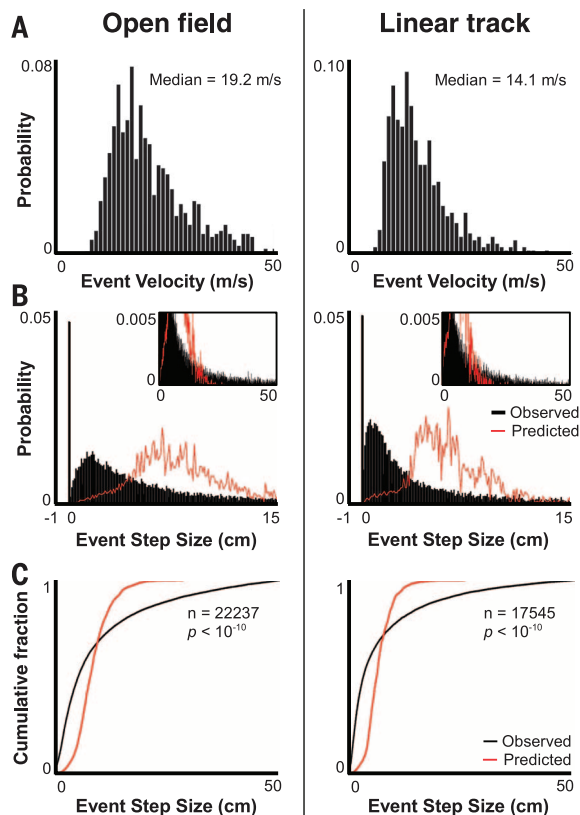
(A) Schematic diagram of the open field (circles indicate reward wells). (B) Behavioral trajectory for rat 1 throughout an entire recording session. (C) Wideband (top) and ripple-filtered (middle) local field potential (LFP), and raster plot of simultaneously recorded neurons (bottom) for a representative SWR in the open arena ± 250 ms. (D) Decoded position (Bayesian posterior probability) for evenly distributed time frames throughout the SWR event in (C). Note that individual frames display a tight, spatially restricted representation.

(E) Mean decoded position across all time frames for the event in (C). Despite spatially localized representations in each individual window (D), the entire SWR encodes a trajectory that crosses the environment. (F) Location (in centimeters) and sequence of the encoded trajectory in the x (top) and y axis (middle) and movement (in centimeters) between each frame (bottom). (G to L) As in (A) to (F), for representative linear track session and trajectory event.

**Fig. 2. Movement during trajectory events.**

Quantification of movement and velocities for trajectories encoded by SWRs during open field (left) and linear track (right) exploration.

(A) Probability histogram (1 m/s bins) of average trajectory event velocities (total distance covered/total event duration). (B and C) Probability histogram (B) (0.1-cm bins) and cumulative distribution (C) of step sizes for all trajectory events. Predicted step sizes (red) based on evenly spaced steps. Inset: zoomed y axis and expanded x axis. Observed versus predicted populations significantly different (Wilcoxon rank-sum test, $P < 10^{-10}$ for both open field and linear track sessions); cumulative distributions significantly different (two-sample Kolmogorov-Smirnov test).



S4). We calculated for each event the step size per frame that would be necessary to encode a smooth trajectory and compared these predicted step sizes to the actual step sizes observed within trajectory events (Fig. 2, B and C). Observed step sizes significantly differed from predicted, with a larger number of very short steps and a longer tail of larger steps (Fig. 2, B and C). The large peak observed at zero arose from consecutive frames in which the spike pattern did not change; eliminating this peak did not affect significance (Wilcoxon rank-sum test, $P < 10^{-10}$ for both open field and linear track sessions). The observation of alternating immobility and movement in trajectory events was observed in two different environments with distinct behavioral requirements and was consistent across a range of decoding criteria, including decoding window size and degree of temporal smoothing (figs. S5 to S9). These data suggest that during SWR-based memory expression, information is not presented in a temporally continuous stream, but is expressed in discrete, temporally separated units. In addition, we observed no effect of trajectory proportion (e.g., start, middle, end) on stepwise movement (fig. S10), indicating that temporal segmentation is present throughout the entirety of a trajectory event and is likely an inherent characteristic of information flow during hippocampal reactivation.

To explore mechanisms underlying the discontinuous flow of information within SWRs, we measured the relative timing of movement and

immobility during trajectory events. We observed that an average stationary epoch lasted 24.1 ± 0.38 ms ($n = 3364$) in open field sessions and 16.7 ± 0.25 ms ($n = 3011$) in linear track sessions, whereas epochs of movement had an average duration of 7.9 ± 0.09 ms ($n = 3324$) and 11.2 ± 0.18 ms ($n = 3060$) in the open field and linear track sessions, respectively. Thus, on average, repeating cycles of immobility and movement occurred at roughly 30 to 40 Hz, prompting us to examine the correlation between information expression in hippocampal reactivation events and the slow-gamma rhythm, a prominent 25- to 50-Hz oscillation that originates in hippocampal area CA3, one synapse upstream from our recording location (11, 12). Consistent with prior reports (13), we noted a transient increase in slow-gamma power during trajectory events (fig. S11). In addition, we observed that both excitatory spiking and movement during trajectory events were phase-locked with the slow-gamma rhythm (Fig. 3, A to C and F to H, and fig. S12). Intriguingly, the preferred phase of movement opposed that of neural activity (Fig. 3, D and I). Accordingly, step size was negatively correlated with spike count during trajectory events (fig. S13), and the total number of spikes across two consecutive decoding windows predicted the result-

ing step size (Fig. 3, E and J). Furthermore, we observed a phase-dependent correlation between movement and the sharpness of decoded position (fig. S14). These results were replicated with multiple decoding criteria and different degrees of temporal smoothing (figs. S15 to S18), suggesting that the correlation of movement with gamma phase was not dependent on the data-binning procedure. Together, these data indicate that the temporal segmentation of trajectory events is governed by slow-gamma oscillations and that during phases of high neuronal activity within the gamma cycle, spatial representation in the hippocampus is often focused on a single location, whereas during phases of low neuronal activity, the spatial representation is more likely to move to adjacent locations.

It might be hypothesized that systematic variation in the measurement process, or in spike number, could account for the correlation between movement and slow-gamma phase. We asked whether it was possible to observe smooth trajectories whose movement was uncorrelated with gamma phase using the data that we had collected and our analysis methods. Without altering place fields or the precise timing of individual spikes (thereby preserving the correlation of in-

dividual spikes to the phase of slow gamma and preserving phase-dependent changes in population firing rate), we created nonrandom shuffles of the cell identities of individual spikes during trajectory events to generate trajectories that followed the same path as the original trajectory event, but progressed smoothly rather than discontinuously through space (fig. S19). The step sizes of these evened trajectory events were not statistically different from ideally smooth step sizes (Fig. 4, A, B, D, and E, and fig. S20). Whereas the correlation of spike activity to slow-gamma rhythm was preserved, the relationship between step size and slow-gamma phase was abolished (Fig. 4, C and F, and fig. S20). We further tested whether our observation of discontinuous movement in trajectory events was a result of poor place-field distribution or inherent noise in neural activity. We simulated trajectory event activity associated with the occupancy of different positions as Poisson spiking based on cells' place fields and the spike rates typically observed during the short time bins used to decode actual trajectory events. We observed that all locations in the arena could be decoded accurately (fig. S21, A and B) and that evenly stepped sequences of positions produced step-size distributions that were significantly

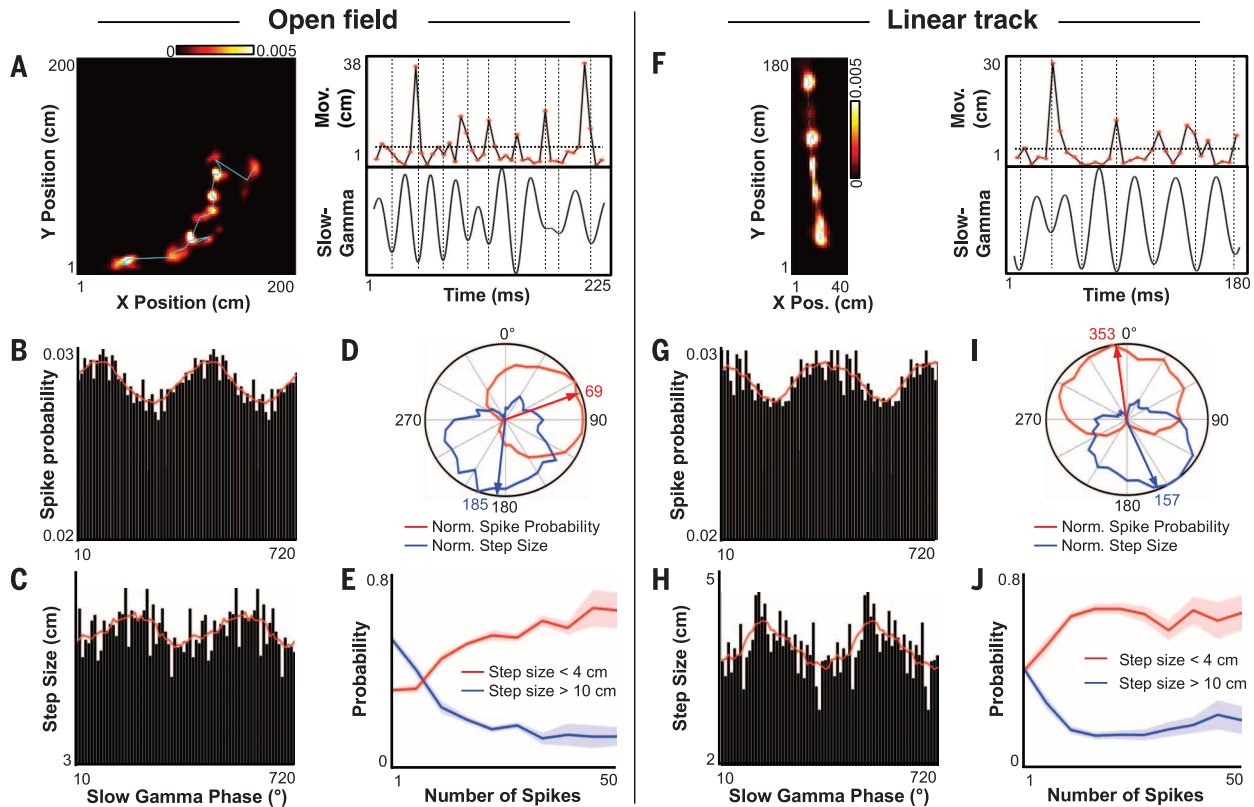
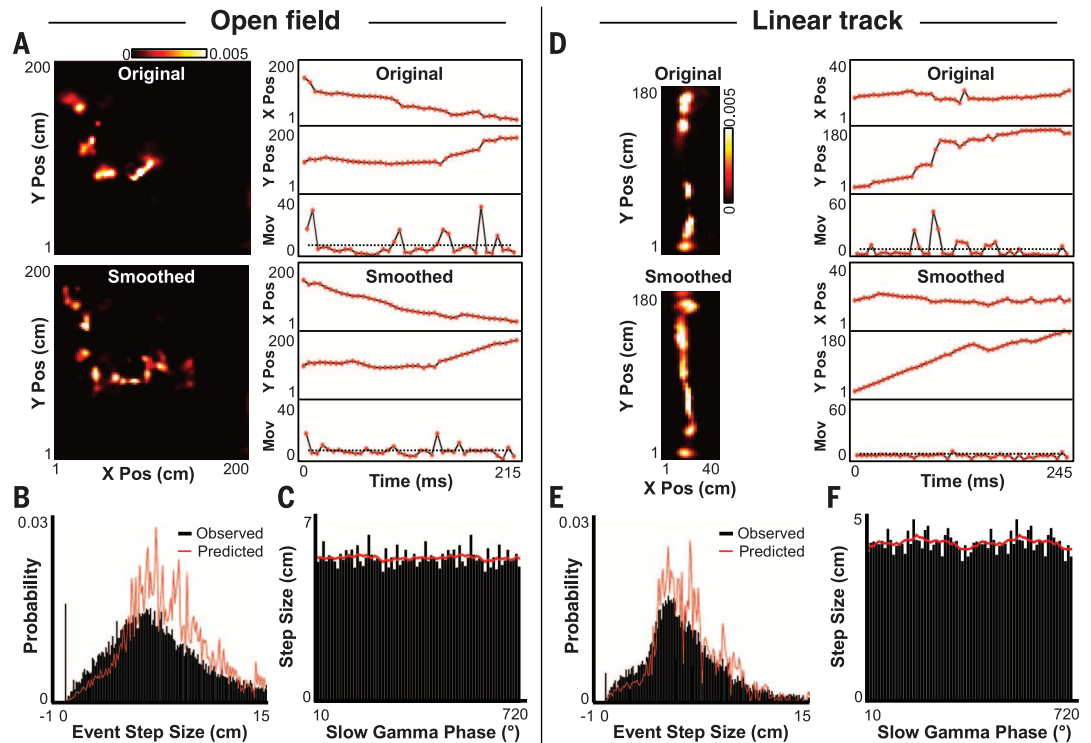


Fig. 3. Correlation between movement, firing rate, and slow-gamma phase. (A) Mean posterior probabilities (left, cyan line indicates temporal sequence), movement (top right), and slow-gamma oscillation (bottom right) for a representative trajectory event. Troughs (180° phase) in the gamma trace indicated with dashed lines. (B and C) For all open field sessions, across-session average spike probability (B) and step size (C) as a function of slow-gamma phase (bin size = 10°) for all trajectory events. Red line indicates running box average (box size = 8 bins). Circular correlation

Monte-Carlo P value (50,000 shuffles of gamma phase): spike probability $P < 2.00 \times 10^{-5}$; step size $P = 4.40 \times 10^{-4}$. (D) Normalized contour plots and circular weighted mean (arrow) for box-average spike probability (red) and step size (blue) as a function of slow-gamma phase. (E) Mean ± SEM probability of observing a step size greater than 10 cm (blue) or less than 4 cm (red) as a function of spike count. (F to J) As in (A) to (E), for linear track events. (G and H) Monte-Carlo P value: spike probability $P < 2.00 \times 10^{-5}$; step size $P < 2.00 \times 10^{-5}$.

Fig. 4. Forced decorrelation of movement and slow-gamma phase.

(A) Representative trajectory event before (top) and after (bottom) spike ID shuffles to smooth the encoded path (fig. S19). (B) Probability histogram of step sizes across all smoothed open field trajectory events. Predicted step sizes (red) based on evenly spaced steps (Fig. 2B). The population of observed step sizes in the smoothed trajectory events not different from predicted (Wilcoxon rank sum test, $P = 0.385$). (C) Across-session average step size as a function of slow-gamma phase (bin size = 10°) for all open field smoothed trajectory events. Red line indicates running box average (box size = 8 bins). No circular correlation observed between smoothed step size and slow-gamma phase (50,000 shuffles of gamma phase, Monte-Carlo P value = 0.632).



(D to F) As in (A) to (C), for linear track sessions. (E) Wilcoxon rank sum test, $P = 0.862$. (F) Monte-Carlo P value = 0.105.

more smooth than actual trajectory events (fig. S21C). Thus, the observation of slow-gamma-locked, discontinuous movement was not a trivial result of our decoding methodology, spike-phase locking, phase-dependent oscillations in population-level firing rate, place-cell sampling, or place-field coverage.

Prior work has demonstrated that slow-gamma power and synchrony across hippocampal areas CA3 and CA1 are transiently increased during both SWRs and memory-dependent tasks (13–15), indicating that these oscillations play a prominent role in memory consolidation and recall processes. Although CA1 recordings cannot conclusively demonstrate the source of observed slow-gamma rhythm (16), it is thought to originate in CA3 (11, 12), a region with a large number of recurrent excitatory connections (17). Several studies are consistent with the notion that this recurrence supports an autoassociative network involved in the mnemonic process of pattern completion (18, 19). It is recognized that unbounded attractor dynamics in such a network can lead to runaway excitatory activity (20). Our data suggest a solution to this problem, in which attractor strength oscillates at the slow-gamma frequency between high levels of activity [focusing neural representation on a “unit” of information (21), such as a single location in space] and low levels of activity (weakening the attractor dynamics to allow transition to a different unit). Our data support the generalization to the SWR state of a model of sequence generation during hippocampal theta, in which a heteroassociative network is identified with connectivity between dentate gyrus and CA3, and an autoassociative network

with recurrent synapses within CA3 (22). Our data further suggest that these processes alternate in time during trajectory-depicting SWR events and that slow-gamma oscillations may govern switching between them. In this way, slow-gamma rhythm may correspond to the passage of information around a multiregional hippocampal loop.

More broadly, our findings of temporal segmentation of information on the scale of the gamma oscillation have implications for memory and information-processing mechanisms in other brain regions. Gamma-frequency rhythms are observed throughout the brain (23), and alterations in gamma oscillations have been linked with several human neuropathies (24). Our data are consistent with a growing body of literature implicating gamma oscillations in general memory functions (14, 25–28). Furthermore, like hippocampal area CA3, many cortical brain regions contain extensive recurrent excitatory connections (29). Rhythmic oscillations are believed to mediate communication and information processing between brain regions by synchronizing local circuitry with remote inputs (30); our data point to an additional role in allowing neuronal architectures to focus representation while avoiding excess positive feedback.

REFERENCES AND NOTES

1. J. J. Hopfield, *Proc. Natl. Acad. Sci. U.S.A.* **79**, 2554–2558 (1982).
2. D. Kleinfeld, *Proc. Natl. Acad. Sci. U.S.A.* **83**, 9469–9473 (1986).
3. H. Sompolinsky, I. Kanter, *Phys. Rev. Lett.* **57**, 2861–2864 (1986).
4. J. O’Neill, T. J. Senior, K. Allen, J. R. Huxter, J. Csicsvari, *Nat. Neurosci.* **11**, 209–215 (2008).
5. T. J. Davidson, F. Kloosterman, M. A. Wilson, *Neuron* **63**, 497–507 (2009).
6. S. P. Jadhav, C. Kemere, P. W. German, L. M. Frank, *Science* **336**, 1454–1458 (2012).
7. G. Buzsáki, *Brain Res.* **398**, 242–252 (1986).

8. M. P. Karlsson, L. M. Frank, *Nat. Neurosci.* **12**, 913–918 (2009).
9. A. S. Gupta, M. A. A. van der Meer, D. S. Touretzky, A. D. Redish, *Neuron* **65**, 695–705 (2010).
10. B. E. Pfeiffer, D. J. Foster, *Nature* **497**, 74–79 (2013).
11. J. Csicsvari, B. Jamieson, K. D. Wise, G. Buzsáki, *Neuron* **37**, 311–322 (2003).
12. L. L. Colgin et al., *Nature* **462**, 353–357 (2009).
13. M. F. Carr, M. P. Karlsson, L. M. Frank, *Neuron* **75**, 700–713 (2012).
14. S. M. Montgomery, G. Buzsáki, *Proc. Natl. Acad. Sci. U.S.A.* **104**, 14495–14500 (2007).
15. A. Johnson, A. D. Redish, *J. Neurosci.* **27**, 12176–12189 (2007).
16. G. Buzsáki, E. W. Schomburg, *Nat. Neurosci.* **18**, 484–489 (2015).
17. X.-G. Li, P. Somogyi, A. Ylänen, G. Buzsáki, *J. Comp. Neurol.* **339**, 181–208 (1994).
18. K. Nakazawa et al., *Neuron* **38**, 305–315 (2003).
19. A. E. Gold, R. P. Kesner, *Hippocampus* **15**, 808–814 (2005).
20. M. E. Hasselmo, E. Schnell, E. Barkai, *J. Neurosci.* **15**, 5249–5262 (1995).
21. J. E. Lisman, M. A. Idiart, *Science* **267**, 1512–1515 (1995).
22. J. E. Lisman, L. M. Talamini, A. Raffone, *Neural Netw.* **18**, 1191–1201 (2005).
23. P. Fries, *Annu. Rev. Neurosci.* **32**, 209–224 (2009).
24. P. J. Uhlhaas, W. Singer, *Neuron* **52**, 155–168 (2006).
25. K. W. Bieri, K. N. Bobbitt, L. L. Colgin, *Neuron* **82**, 670–681 (2014).
26. K. M. Igarashi, L. Lu, L. L. Colgin, M.-B. Moser, E. I. Moser, *Nature* **510**, 143–147 (2014).
27. R. T. Canolty et al., *Science* **313**, 1626–1628 (2006).
28. P. R. Shirvvalkar, P. R. Rapp, M. L. Shapiro, *Proc. Natl. Acad. Sci. U.S.A.* **107**, 7054–7059 (2010).
29. R. J. Douglas, K. A. Martin, *Annu. Rev. Neurosci.* **27**, 419–451 (2004).
30. J. Lisman, *Hippocampus* **15**, 913–922 (2005).

ACKNOWLEDGMENTS

We thank K. Zhang for discussion. This work was supported by the National Institute for Mental Health (D.J.F.). The data described in this manuscript are stored in the laboratory of D.J.F. in the Department of Neuroscience, Johns Hopkins University.

SUPPLEMENTARY MATERIALS

www.sciencemag.org/content/349/6244/180/suppl/DC1
Materials and Methods
Figs. S1 to S22

20 February 2015; accepted 21 May 2015
10.1126/science.aaa9633

This copy is for your personal, non-commercial use only.

If you wish to distribute this article to others, you can order high-quality copies for your colleagues, clients, or customers by [clicking here](#).

Permission to republish or repurpose articles or portions of articles can be obtained by following the guidelines [here](#).

The following resources related to this article are available online at www.sciencemag.org (this information is current as of July 23, 2015):

Updated information and services, including high-resolution figures, can be found in the online version of this article at:

<http://www.sciencemag.org/content/349/6244/180.full.html>

Supporting Online Material can be found at:

<http://www.sciencemag.org/content/suppl/2015/07/08/349.6244.180.DC1.html>

This article **cites 30 articles**, 9 of which can be accessed free:

<http://www.sciencemag.org/content/349/6244/180.full.html#ref-list-1>

This article appears in the following **subject collections**:

Neuroscience

<http://www.sciencemag.org/cgi/collection/neuroscience>